

Structural and Dynamical Properties of NaBH₄ and KBH₄: NMR and Synchrotron X-ray Diffraction Studies

Olga A. Babanova,[†] Alexei V. Soloninin,[†] Adolf P. Stepanov,[†] Alexander V. Skripov,^{*,†} and Yaroslav Filinchuk^{*,‡}

Institute of Metal Physics, Ural Division of the Russian Academy of Sciences, S. Kovalevskoi 18, Ekaterinburg 620041, Russia, and Swiss-Norwegian Beam Lines at ESRF, 6 rue Horowitz, BP-220, 38043, Grenoble, France

Received: December 18, 2009; Revised Manuscript Received: January 29, 2010

The temperature dependence of the structural parameters of NaBH₄ has been investigated by synchrotron X-ray diffraction over the range of 80–500 K. On the basis of the diffraction data, we revise the structure of the low-temperature (tetragonal) phase of NaBH₄ and discuss the changes in the lattice parameters and the patterns of H···H contacts in the low-*T* and high-*T* phases. To study the atomic motion in NaBH₄ and KBH₄, we have performed nuclear magnetic resonance (NMR) measurements of the ¹H and ¹¹B spin–lattice relaxation rates in these compounds over wide ranges of temperature (82–424 K) and resonance frequency (14–90 MHz). For both compounds, the NMR results are governed by the thermally activated reorientational motion of the BH₄ groups, and the changes in the jump rates of reorientations are traced over the range of 8 orders of magnitude. The activation energies of the reorientational motion are found to be equal to 0.151 ± 0.002 eV (low-*T* phase of NaBH₄), 0.126 ± 0.003 eV (high-*T* phase of NaBH₄), and 0.161 ± 0.002 eV (high-*T* phase of KBH₄). Structural changes in the series of alkali metal borohydrides are analyzed in connection with the changes in the phase-transition temperature, the compressibility, and the barrier of the reorientational BH₄ motion. On the basis of this analysis, we discuss the role of different interatomic interactions in determining the physical properties of alkali metal borohydrides.

Introduction

Alkali metal borohydrides MBH₄ (M = alkali metal) are considered as promising materials for hydrogen storage.^{1,2} Although the volumetric and gravimetric hydrogen densities in these compounds are high, the stability of the borohydrides with respect to thermal decomposition and the slow sorption kinetics remain the major drawbacks for their practical use. Elucidation of the complex structures and hydrogen dynamics in these materials may give a key to improving their hydrogen-storage properties by the inclusion of catalytic or destabilizing additives. Alkali metal borohydrides form ionic crystals consisting of M⁺ cations and tetrahedral [BH₄][−] anions. The structural aspects of light metal borohydrides have been recently reviewed in ref 3.

At ambient pressure, the prospective hydrogen-storage compound NaBH₄^{4,5} can exist in two structural modifications. The high-temperature phase of NaBH₄ is cubic; it contains orientationally disordered BH₄ groups,⁶ and its structure should be described in the space group *Fm* $\bar{3}$ *m*.^{7,8} On cooling below *T*₀ ≈ 190 K, the cubic phase transforms to the closely related ordered tetragonal phase.⁹ The same tetragonal phase can also be obtained by applying a pressure of ~6 GPa at room temperature.^{10,11} The high-temperature cubic phase of KBH₄^{12,13} is isomorphous to that of NaBH₄. However, for KBH₄, the transition to the ordered tetragonal phase is observed at a much lower temperature (*T*₀ ≈ 70 K).¹³

The aims of the present work are to study the temperature dependences of the structural parameters for NaBH₄ and the reorientational motion of BH₄ groups in NaBH₄ and KBH₄. The structural part of this work employs the synchrotron X-ray powder diffraction measurements over the temperature range of 80–500 K. Diffraction study of the temperature evolution of NaBH₄ has not been reported so far. On the basis of our diffraction data, we revise the structure of the low-*T* phase of NaBH₄ and discuss the changes in the lattice parameters and the patterns of H···H contacts in the low-*T* and high-*T* phases. To investigate the atomic motion in NaBH₄ and KBH₄, we use nuclear magnetic resonance (NMR) measurements of the ¹H and ¹¹B spin–lattice relaxation rates *R*₁ over the temperature range of 82–424 K. Previous NMR measurements of *R*₁ for NaBH₄^{14–16} and KBH₄¹⁴ were interpreted in terms of the thermally activated reorientational motion of BH₄ groups. Other techniques used to characterize the reorientational motion in NaBH₄ and KBH₄ include Raman scattering^{13,17} and quasielastic neutron scattering (QENS) measurements for the high-*T* phase of NaBH₄.¹⁸ It should be noted that each of the previous NMR studies of the BH₄ reorientations in NaBH₄ and KBH₄ was performed at a single resonance frequency. However, to characterize complex atomic motions, it is often important to investigate the frequency dependence of *R*₁. Such an approach can be used to search for a distribution of atomic jump rates¹⁹ or a coexistence of several types of jump motion with different rates.²⁰ Our *R*₁ measurements have been performed over a wide range of the resonance frequencies (14–90 MHz). The temperature range of our *R*₁ measurements is also substantially wider than in the previous NMR experiments; this is expected to result in the higher precision of the activation energies obtained from the data. Apart from deriving the parameters of the reorienta-

* To whom correspondence should be addressed. E-mail: skripov@imp.uran.ru (A.V.S.), yaroslav.filinchuk@esrf.fr (Y.F.). Fax: +7-343-374-5244 (A.V.S.), +33-47-688-2694 (Y.F.).

[†] Ural Division of the Russian Academy of Sciences.

[‡] Swiss-Norwegian Beam Lines at ESRF.

tional motion in NaBH₄ and KBH₄, our discussion of the NMR data addresses the following questions: (1) are there any distributions of the jump rates for the BH₄ reorientations, and (2) are there any signs of the *long-range* diffusion of cations or anions on the NMR frequency scale (as in the case of LiBH₄^{21–25})? We also discuss the role of interatomic interactions in determining the physical properties of alkali metal borohydrides.

Experimental Methods

NaBH₄ and KBH₄ with a nominal purity of 98% and 99.9%, respectively, were purchased from Sigma-Aldrich. Diffraction data for the polycrystalline NaBH₄ were collected at the Swiss-Norwegian Beam Lines (BM1A) of the European Synchrotron Radiation Facility (ESRF) in Grenoble. A MAR345 imaging plate detector at the sample-to-detector distance of 120 mm and the synchrotron radiation with the wavelength $\lambda = 0.716698 \text{ \AA}$ were used. A 0.5 mm glass capillary filled in a high-purity Ar atmosphere with a fine powder of NaBH₄ was cooled from room temperature to 100 K and then heated up to 500 K at a rate of 60 K/h, while synchrotron powder diffraction data were collected in situ. The temperature was controlled with an Oxford Cryostream 700+. Each pattern was collected during 30 s exposure time, while the capillary was rotated by 30°, followed by a readout during 83 s. The data were integrated using the Fit2D program²⁶ and a calibration measurement of an NIST LaB₆ standard sample. Highly accurate integrated intensities were obtained thanks to a good powder average achieved by projecting the 3D scattering information on the 2D detector. Uncertainties of the integrated intensities were calculated at each 2θ -point by applying Poisson statistics to the intensity data, considering the geometry of the detector, similar to the procedure described in ref 27. The calculated absorption effect is negligible; thus, the absorption correction was not applied. Structural models for the high-temperature cubic and the low-temperature tetragonal phases of NaBH₄ were taken, respectively, from refs 8 and 9. For the latter case, we revised the originally proposed $P\bar{4}2_1c$ structure (see the Results and Discussion) in the higher symmetry, $P4_2/nmc$. The structures were refined by the Rietveld method using the Fullprof program.²⁸ One coordinate parameter was refined for the cubic phase, and two for the tetragonal phase, in both cases, for the hydrogen atoms. Isotropic atomic displacements for Na, B, and H atoms were refined independently, for both phases. Peak shapes were described by the pseudo-Voigt function, and the 2θ dependence of peak width was parametrized by the Caglioti formula. The background was described by a linear interpolation between selected points. All the 237 data sets measured with an $\sim 2.4 \text{ K}$ step were treated by a sequential refinement in Fullprof.²⁸ The refinements converged at $R_B = 2\text{--}3\%$, $R_F = 1.5\text{--}2\%$, $R_p = 5\%$, and $R_{wp} = 4\text{--}5\%$.

For NMR experiments, powdered samples of NaBH₄ and KBH₄ were sealed in glass tubes under nitrogen gas. NMR measurements were performed on a modernized Bruker SXP pulse spectrometer with quadrature phase detection at the frequencies $\omega/2\pi = 14, 23.8,$ and 90 MHz (for ¹H) and 14 and 28 MHz (for ¹¹B). The magnetic field was provided by a 2.1 T iron-core Bruker magnet. A home-built multinuclear continuous-wave NMR magnetometer working in the range of 0.32–2.15 T was used for field stabilization. For rf pulse generation, we used a home-built computer-controlled pulse programmer, the PTS frequency synthesizer (Programmed Test Sources, Inc.), and a 1 kW Kalmus wideband pulse amplifier. Typical values of the $\pi/2$ pulse length were 2–3 μs for both ¹H and ¹¹B. A probe head with the sample was placed into an Oxford

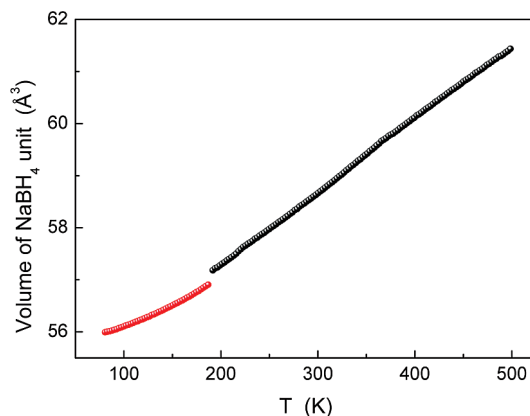


Figure 1. Volume of NaBH₄ formula unit versus temperature; a 0.4% volume increase is observed upon the transition to the cubic phase.

Instruments CF1200 continuous-flow cryostat using nitrogen as a cooling agent. The sample temperature, monitored by a chromel–(Au–Fe) thermocouple, was stable to $\pm 0.1 \text{ K}$. The nuclear spin–lattice relaxation rates were measured using the saturation–recovery method. In all cases, the recovery of the nuclear magnetization could be satisfactorily described by a single exponential function. NMR spectra were recorded by Fourier transforming the spin-echo signals.

Results and Discussion

1. NaBH₄: Temperature Evolution from Synchrotron X-ray Diffraction Data. The tetragonal structure was originally reported in the space group $P\bar{4}2_1c$, but it was pointed out²⁹ that the structure deviates insignificantly from the higher symmetry, $P4_2/nmc$. Our refinements and analysis show that the true symmetry of the tetragonal structure is indeed $P4_2/nmc$. The two space groups differ with respect to the set of reflections $hk0$: reflections with the even sum $h + k$ should be observed in $P\bar{4}2_1c$ and systematically absent in $P4_2/nmc$. The 2θ positions for the Bragg reflections 210, 320, 410, 430, and 520 are well-separated from other peaks, but they are not observable from our powder data. We note that the very high counting statistics of the area detector allowed us to define accurately the background and reliably detect even very weak diffraction peaks. The fit to the diffraction data using a slightly simpler $P4_2/nmc$ model results in practically the same values of the reliability factors. Thus, we revise the tetragonal structure of NaBH₄ in the space group $P4_2/nmc$.

A hypothesis of a partial disorder of the BH₄ group in the $P4_2/nmc$ structure by a 90° rotation around the 4_2 axis has been examined by refining the occupancies corresponding to the two alternative BH₄ orientations. It showed that, at all temperatures, from 80 K up to the transition at $\sim 187 \text{ K}$, the BH₄ group is fully ordered. Thus, the order–disorder phenomenon in NaBH₄ occurs abruptly upon the transition to the cubic phase. The crystallographic details for the revised structure at 180 K are listed in the Supporting Information (Table S1 and Figure S1).

The tetragonal phase transforms into the cubic one at $\sim 187 \text{ K}$, and the transition is accompanied by a 0.4% volume increase (see Figure 1). For the cubic phase, in the 190–500 K range, the volume of the NaBH₄ formula unit, V/Z (\AA^3), can be well approximated by a simple linear equation: $V/Z = 54.470(8) + 1.406(2) \cdot 10^{-2} T$. For the tetragonal phase, in the 80–190 K range, the dependence is nearly quadratic: $V/Z = 55.785(1) + 2.99(5) \cdot 10^{-5} T^2$, where the linear part was negligible and thus set to zero. As can be seen from the slopes in Figure 1, the volumetric expansion coefficients for the two phases at 187 K

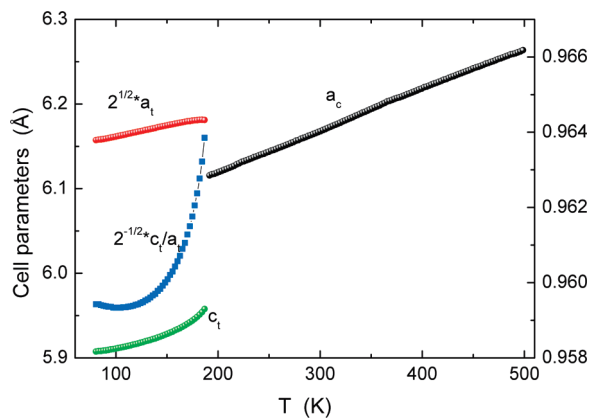


Figure 2. Temperature dependence of the cell parameters for NaBH₄ obtained from the in situ powder diffraction data. The *c/a* ratio for the pseudocubic cell is shown by blue squares, with the scale indicated on the right axis.

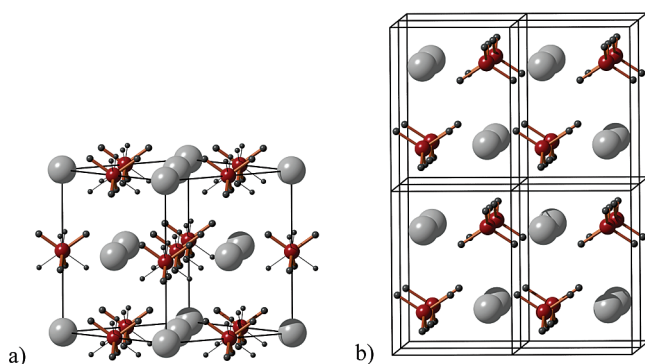


Figure 3. Crystal structure of NaBH₄ phases: *Fm* $\bar{3}m$ (a) and *P4*₂/*nmc* (b). Two orientations of the disordered BH₄ group in the cubic phase are shown by bold and thin lines.

($1/V_{187\text{ K}} \times dV/dT$) are significantly different: $1.96 \times 10^{-4} \text{ K}^{-1}$ for the tetragonal and $2.46 \times 10^{-4} \text{ K}^{-1}$ for the cubic phase. Thus, the transition from the tetragonal to the cubic phase is accompanied both by the small volume increase and by a 25% increase in the volumetric expansion coefficient.

The cell parameters for the two NaBH₄ phases, extracted from the sequential Rietveld refinement, are plotted in Figure 2. Thermal expansion of the tetragonal phase is anisotropic, especially close to the transition temperature. The *c/a* ratio of the pseudocubic cell is considerably lower than the ideal ratio of 1 for the cubic phase. On the transition at 187 K, it drops from 1 to 0.964 and continues to decrease, reaching a minimum at slightly over 100 K. The change in the *c/a* ratio is primarily achieved by the contraction of the tetragonal *c* axis and, to a smaller extent, by the expansion in the basal plane.

The cubic and the tetragonal phases are closely related; Na atoms and BH₄ groups are octahedrally coordinated in both structures (Figure 3). Apart from the tetragonal deformation of the low-temperature phase, the two structures, first of all, differ by the patterns of H \cdots H contacts. The shortest repulsive H \cdots H interactions between the adjacent BH₄ groups in the cubic phase favor the disorder: their number in the disordered *Fm* $\bar{3}m$ structure is half of that in a hypothetical ordered *F* $\bar{4}3m$ structure.^{3,7} As the temperature is lowered, the H \cdots H distances become shorter (see Figure S2 of the Supporting Information), increasing the repulsion. Lowering the lattice symmetry in the tetragonal phase allows ordering of the BH₄ groups in a different way so that the number of the shortest H \cdots H contacts is further reduced by one-third, while keeping the H \cdots H distances nearly

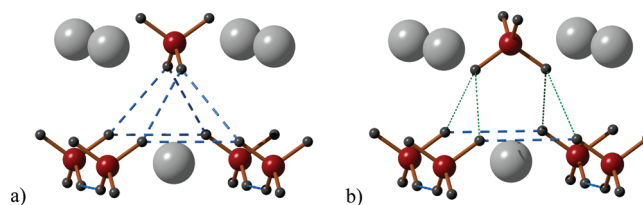


Figure 4. Configuration of the maximal BH₄ \cdots BH₄ repulsion, statistically occurring in the cubic phase (a), and an ordered pattern involving longer H \cdots H contacts in the tetragonal phase (b). The blue dashed and green dotted lines indicate the first and the second shortest H \cdots H distances. The *c* axis is oriented vertically.

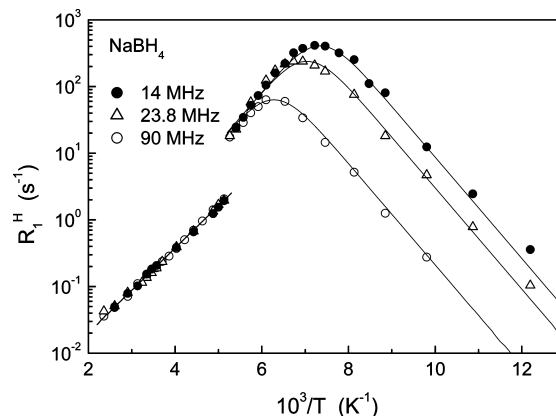


Figure 5. Proton spin–lattice relaxation rates measured at 14, 23.8, and 90 MHz for NaBH₄ as a function of the inverse temperature. The solid lines show the simultaneous fits of the model based on eqs 1 and 2 to the data.

unaffected (see Figure S2 of the Supporting Information). As a result of this scheme, an isotropic disordered three-dimensional (3D) network of the repulsive H \cdots H contacts in the cubic phase transforms into an ordered two-dimensional (2D) network, oriented in the *ab* plane of the tetragonal cell. Figure 4a shows the configuration of the maximum BH₄ \cdots BH₄ repulsion, statistically occurring in the cubic phase, compared with the less repulsive ordered pattern involving longer H \cdots H contacts in the tetragonal phase (Figure 4b). The ordering of the BH₄ groups induces the tetragonal distortion, seen as the abrupt drop of the *c/a* ratio (Figure 2). Above 300 K, the atomic displacement parameters (ADPs) extracted from the Rietveld refinements increase almost linearly with the temperature, and below 300 K, the temperature dependence of the ADPs deviates from the linear behavior (see Figure S3 of the Supporting Information), approaching their low-temperature limits.³⁰ As can be seen from Figure S3 (Supporting Information), the ordering at 187 K is accompanied by a small drop of the ADPs for the BH₄ groups.

2. NaBH₄: ¹H and ¹¹B Spin–Lattice Relaxation Data. The temperature dependences of the proton spin–lattice relaxation rates R_1^H measured at three resonance frequencies $\omega/2\pi$ for NaBH₄ are shown in Figure 5. The general features of the observed behavior of R_1^H are typical of the relaxation mechanism due to nuclear dipole–dipole interaction modulated by thermally activated atomic motion.³¹ Because the measured width of the proton NMR line at half-maximum remains to be about 28 kHz over the temperature range of 110–424 K, this motion should be localized. It can be identified as reorientations of the BH₄ tetrahedra. For the low-temperature (tetragonal) phase of NaBH₄, the proton relaxation rate shows the frequency-dependent peak (Figure 5) at the temperature at which the reorientation jump rate τ^{-1} becomes nearly equal to ω . The first-order phase transition from the tetragonal to the cubic phase near 190 K is

accompanied by the sharp decrease in the proton spin–lattice relaxation rate (Figure 5). This decrease in R_1^H corresponds to nearly an order of magnitude *increase* in the reorientation jump rate τ^{-1} because, at the high-temperature slope of the relaxation rate peak, R_1^H is proportional³¹ to τ (see eq 1 below). For the high-temperature (cubic) phase, the measured relaxation rates are frequency-independent (Figure 5); this shows that, for the cubic phase, the values of τ^{-1} are much higher than ω . The experimental results have been described in terms of the standard expressions for the motionally induced relaxation³¹ with the Arrhenius-type temperature dependence of τ^{-1} . To estimate the relative strength of the ^1H – ^{11}B , ^1H – ^1H , and ^1H – ^{23}Na dipole–dipole interactions, we have calculated the corresponding contributions to the “rigid lattice” second moment of the ^1H NMR line on the basis of the structural data, taking into account internuclear distances up to 4 Å. The resulting “rigid lattice” contributions for the tetragonal phase are $M_{\text{HB}}^R = 1.44 \times 10^{10} \text{ s}^{-2}$, $M_{\text{HH}}^R = 1.68 \times 10^{10} \text{ s}^{-2}$, and $M_{\text{HNa}}^R = 4.69 \times 10^8 \text{ s}^{-2}$. For the cubic phase, these contributions remain nearly unchanged ($1.44 \times 10^{10} \text{ s}^{-2}$, $1.69 \times 10^{10} \text{ s}^{-2}$, and $4.56 \times 10^8 \text{ s}^{-2}$, respectively). Thus, the H–B and H–H interactions are of approximately equal strength, whereas the H–Na interactions are more than an order of magnitude weaker. Therefore, the proton spin–lattice relaxation rate is dominated by the sum of contributions due to H–B and H–H dipole–dipole interactions

$$R_1^H = \frac{\Delta M_{\text{HB}} \tau}{2} \left[\frac{1}{1 + (\omega_{\text{H}} - \omega_{\text{B}})^2 \tau^2} + \frac{3}{1 + \omega_{\text{H}}^2 \tau^2} + \frac{6}{1 + (\omega_{\text{H}} + \omega_{\text{B}})^2 \tau^2} \right] + \frac{4\Delta M_{\text{HH}} \tau}{3} \left[\frac{1}{4 + \omega_{\text{H}}^2 \tau^2} + \frac{1}{1 + \omega_{\text{H}}^2 \tau^2} \right] \quad (1)$$

where ω_{H} and ω_{B} are the resonance frequencies of ^1H and ^{11}B , respectively, and ΔM_{HB} and ΔM_{HH} are the parts of the dipolar second moment due to H–B and H–H interactions that are caused to fluctuate by the localized atomic motion. We assume that the temperature dependence of τ^{-1} is governed by the Arrhenius law

$$\tau^{-1} = \tau_0^{-1} \exp(-E_a/k_{\text{B}}T) \quad (2)$$

where E_a is the activation energy of the reorientational motion. The parameters of the model are ΔM_{HB} , ΔM_{HH} , τ_0 , and E_a . These parameters are varied to find the best fit to the $R_1^H(T)$ data at the three resonance frequencies simultaneously. Because the H–B and H–H terms in eq 1 show nearly the same temperature and frequency dependences, it is practically impossible to determine independently the amplitude parameters ΔM_{HB} and ΔM_{HH} from the fits. Therefore, we have to assume that the ratio $\Delta M_{\text{HB}}/\Delta M_{\text{HH}}$ is nearly the same as for the corresponding contributions to the “rigid lattice” dipolar second moment.

The results of the simultaneous fit based on eqs 1 and 2 are shown by solid curves in Figure 5. As can be seen from this figure, for the low-temperature (tetragonal) phase of NaBH₄, the model gives an excellent description of the experimental data at three resonance frequencies. In contrast to the case of LiBH₄,²² we have not found any signs of two coexisting types of reorientational motion with different jump rates. The existence of a continuous distribution of the jump rates can also be excluded. In fact, such a distribution would make the frequency dependence of R_1^H substantially weaker¹⁹ than that predicted by

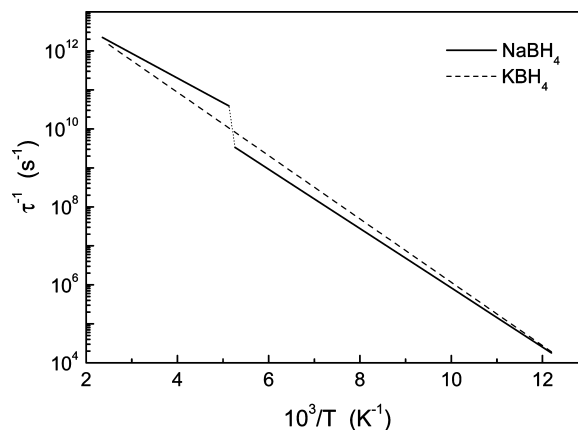


Figure 6. Temperature dependences of the jump rates for BH₄ group reorientations, as derived from the fits to the proton spin–lattice relaxation data for NaBH₄ and KBH₄.

the standard model. For the tetragonal phase, the values of the amplitude parameters resulting from the fits are $\Delta M_{\text{HB}} = 1.1 \times 10^{10} \text{ s}^{-2}$ and $\Delta M_{\text{HH}} = 1.25 \times 10^{10} \text{ s}^{-2}$, and the corresponding motional parameters are $\tau_0 = (3.0 \pm 0.1) \times 10^{-14} \text{ s}$ and $E_a = 0.151 \pm 0.002 \text{ eV}$ (or $14.6 \pm 0.2 \text{ kJ/mol}$). Our result for the activation energy in the tetragonal phase is in reasonable agreement with those of the previous NMR studies ($14.8 \pm 0.7 \text{ kJ/mol}^{14}$ and $15.3 \pm 0.4 \text{ kJ/mol}^{16}$).

For the high-temperature (cubic) phase of NaBH₄, the measured proton spin–lattice relaxation rates do not show any peak. Because of this feature, only the activation energy can be directly derived from the data. Additional assumptions are necessary to determine the pre-exponential factor τ_0 . Tsang and Farrar¹⁴ implicitly assumed that the value of τ_0 for the cubic phase is the same as that for the tetragonal phase. However, this assumption is difficult to justify. In our analysis, we assume that the amplitude parameters ΔM_{HB} and ΔM_{HH} for the cubic phase are the same as the corresponding parameters for the tetragonal phase. This assumption is supported by our calculations of the second moments for the two phases (see above). For the cubic phase, the values of the motional parameters resulting from our fit are $\tau_0 = (1.4 \pm 0.2) \times 10^{-14} \text{ s}$ and $E_a = 0.126 \pm 0.003 \text{ eV}$ (or $12.2 \pm 0.3 \text{ kJ/mol}$). Our result for the activation energy in the cubic phase is in reasonable agreement with those of the NMR study¹⁴ ($11.2 \pm 0.5 \text{ kJ/mol}$) and the quasielastic neutron scattering study¹⁸ ($0.117 \pm 0.001 \text{ eV}$) but disagrees with that of the NMR work¹⁶ ($14.8 \pm 0.4 \text{ kJ/mol}$). It should be noted that, in contrast to refs 14 and 16, our analysis for both phases is based on the data at three resonance frequencies and includes broader ranges of the temperature and R_1^H values. The temperature dependence of the jump rate τ^{-1} resulting from our fits is shown in Figure 6 in the form of an Arrhenius plot. The temperature range of the lines in this figure corresponds to the range of our $R_1^H(T)$ data. As can be seen from Figure 6, the proton spin–lattice relaxation measurements allow one to trace the changes in the jump rate of reorientations in NaBH₄ over the range of 8 orders of magnitude. However, it is difficult to identify the type of reorientations (2-fold or 3-fold jump rotations of the BH₄ tetrahedra) on the basis of the spin–lattice relaxation measurements. As discussed in ref 22, the calculated values of ΔM_{HB} and ΔM_{HH} for the 2-fold and 3-fold reorientations of an isolated BH₄ group appear to be close to each other. In contrast to the case of LiBH₄,^{21–24} our proton NMR measurements have not revealed any signs of translational diffusion of Na ions or BH₄ groups in NaBH₄ up to 424 K. As noted above, the observed width of the proton NMR line in

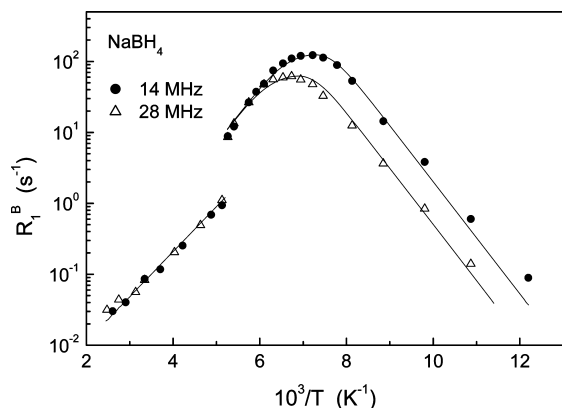


Figure 7. ^{11}B spin–lattice relaxation rates measured at 14 and 28 MHz for NaBH_4 as a function of the inverse temperature. The solid lines show the simultaneous fits of the model based on eqs 3 and 2 to the data.

NaBH_4 remains nearly constant (28 kHz) over the temperature range of 110–424 K. This suggests that the rate of atomic jumps leading to translational diffusion remains below $\sim 10^5 \text{ s}^{-1}$ up to 424 K.

The temperature dependences of the ^{11}B spin–lattice relaxation rates R_1^{B} measured at two resonance frequencies for NaBH_4 are shown in Figure 7. Comparison of Figures 5 and 7 indicates that the general features of the behavior of the ^{11}B relaxation rates are similar to those of the proton relaxation rates. As in the case of LiBH_4 ,²² the quadrupole contribution to the ^{11}B relaxation rate in NaBH_4 should be small, and the dominant contribution to this rate originates from the B–H dipole–dipole interaction modulated by reorientations of the BH_4 tetrahedra. This dominant contribution can be written as

$$R_1^{\text{B}} = \frac{\Delta M_{\text{BH}} \tau}{2} \left[\frac{1}{1 + (\omega_{\text{B}} - \omega_{\text{H}})^2 \tau^2} + \frac{3}{1 + \omega_{\text{B}}^2 \tau^2} + \frac{6}{1 + (\omega_{\text{B}} + \omega_{\text{H}})^2 \tau^2} \right] \quad (3)$$

where ΔM_{BH} is the part of the ^{11}B dipolar second moment due to B–H interaction that is caused to fluctuate by the localized atomic motion. The results of the simultaneous fit of eqs 3 and 2 to the $R_1^{\text{B}}(T)$ data at two resonance frequencies are shown by solid lines in Figure 7. For the tetragonal phase, the resulting parameters are $\Delta M_{\text{BH}} = 1.1 \times 10^{10} \text{ s}^{-2}$, $\tau_0 = (1.5 \pm 0.2) \times 10^{-14} \text{ s}$, and $E_a = 0.157 \pm 0.003 \text{ eV}$ (or $15.1 \pm 0.3 \text{ kJ/mol}$). As in the case of the ^1H spin–lattice relaxation rate, we assume here that the amplitude parameter ΔM_{BH} for the cubic phase is the same as for the tetragonal phase. The resulting motional parameters for the cubic phase are $\tau_0 = (1.1 \pm 0.3) \times 10^{-14} \text{ s}$ and $E_a = 0.126 \pm 0.003 \text{ eV}$ (or $12.2 \pm 0.3 \text{ kJ/mol}$). Note that, for both phases, the E_a values derived from the ^{11}B relaxation data are close to those obtained from the ^1H relaxation data. This may serve as additional evidence for the reliability of our values of the activation energies for the reorientational motion in NaBH_4 .

3. KBH_4 : ^1H and ^{11}B Spin–Lattice Relaxation Data. The temperature dependences of the proton spin–lattice relaxation rates measured at three resonance frequencies for KBH_4 are shown in Figure 8. In contrast to the case of NaBH_4 , the $R_1^{\text{H}}(T)$ dependence for KBH_4 does not show any jump in the studied temperature range of 82–424 K. In fact, the temperature of the structural phase transition for KBH_4 ($\sim 70 \text{ K}$) is below this range.

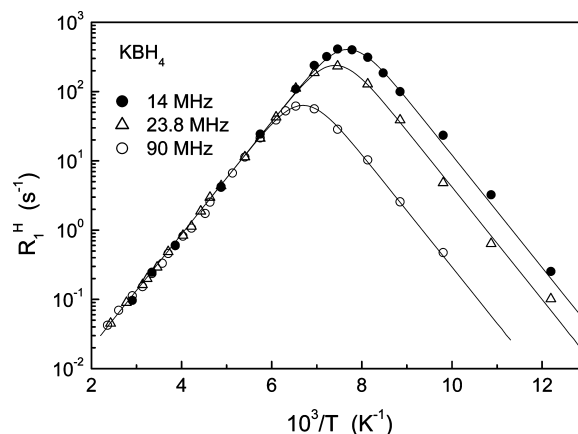


Figure 8. Proton spin–lattice relaxation rates measured at 14, 23.8, and 90 MHz for KBH_4 as a function of the inverse temperature. The solid lines show the simultaneous fits of the model based on eqs 1 and 2 to the data.

Therefore, all of our relaxation rate data for KBH_4 correspond to the high-temperature (cubic) phase. The ^1H – ^{39}K contribution to the second moment of the proton NMR line in KBH_4 is considerably smaller than the corresponding ^1H – ^{23}Na contribution in NaBH_4 . Thus, we can safely neglect the H–K contribution to the proton relaxation rate and use the same eq 1 for the description of the $R_1^{\text{H}}(T)$ data for KBH_4 . The solid lines in Figure 8 show the results of the fit of eqs 1 and 2 to the proton spin–lattice relaxation data at the three resonance frequencies simultaneously. The amplitude parameters resulting from the fit are $\Delta M_{\text{HB}} = 1.1 \times 10^{10} \text{ s}^{-2}$ and $\Delta M_{\text{HH}} = 1.25 \times 10^{10} \text{ s}^{-2}$. These values are the same as the corresponding values for NaBH_4 . The motional parameters resulting from the fit for KBH_4 are $\tau_0 = (6.5 \pm 0.5) \times 10^{-15} \text{ s}$ and $E_a = 0.161 \pm 0.002 \text{ eV}$ (or $15.5 \pm 0.2 \text{ kJ/mol}$). The value of E_a reported in ref 14 for KBH_4 is $14.8 \pm 0.4 \text{ kJ/mol}$. Comparison of the activation energies for the reorientational motion in the isomorphous cubic phases of KBH_4 and NaBH_4 shows that the value of E_a for KBH_4 is considerably higher than that for NaBH_4 . This difference may be related to the difference in the unit cell volumes. The temperature dependence of the jump rate τ^{-1} resulting from our fit for KBH_4 is shown by the dashed line in Figure 6. As can be seen from this figure, despite the difference in activation energies, the reorientation rates τ^{-1} for KBH_4 and NaBH_4 appear to be nearly the same at the high-temperature limit of our $R_1^{\text{H}}(T)$ measurements.

Figure 9 shows the temperature dependences of the ^{11}B spin–lattice relaxation rates for KBH_4 measured at two resonance frequencies. As in the case of the ^{11}B relaxation rates for NaBH_4 , our analysis is based on eqs 3 and 2. The results of the simultaneous fit of these equations to the experimental data at two frequencies are shown by solid lines in Figure 9. The amplitude parameter resulting from the fit, $\Delta M_{\text{BH}} = 1.1 \times 10^{10} \text{ s}^{-2}$, is the same as the corresponding parameter for NaBH_4 . This is not surprising because ΔM_{BH} is determined mainly by the B–H distance in a BH_4 tetrahedron, and this distance is the same for NaBH_4 and KBH_4 . The motional parameters resulting from the fit for ^{11}B in KBH_4 are $\tau_0 = (4.6 \pm 0.5) \times 10^{-15} \text{ s}$ and $E_a = 0.161 \pm 0.003 \text{ eV}$ (or $15.5 \pm 0.3 \text{ kJ/mol}$). Note that this value of the activation energy is the same as that found from our ^1H relaxation data for KBH_4 . As in the case of NaBH_4 , for KBH_4 , we have not found any signs of distributions of jump rates for the reorientational motion or any signs of translational diffusion on the NMR frequency scale.

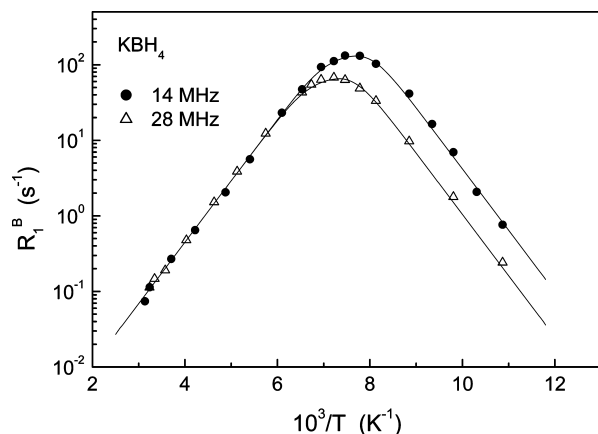


Figure 9. ¹¹B spin–lattice relaxation rates measured at 14 and 28 MHz for KBH₄ as a function of the inverse temperature. The solid lines show the simultaneous fits of the model based on eqs 3 and 2 to the data.

4. Role of Interatomic Interactions in Determining the Physical Properties of MBH₄. The cubic KBH₄ undergoes the same transition to the low-temperature phase as NaBH₄, but at a lower temperature of ~ 70 K.¹³ Because the transition is driven by reducing the number of repulsive H \cdots H interactions, we can conclude that they are weaker in the case of KBH₄. Indeed, the larger potassium ions allow a bigger space between the BH₄ anions. Because the free energies of the disordered cubic and the ordered tetragonal phases should be equal at the transition temperature, the enthalpy difference between these phases is $k_B T_0 \ln 2$. Thus, it is $187/70 \approx 2.7$ times lower for KBH₄ than for NaBH₄. This enthalpy difference between the two phases is still lower for RbBH₄, which does not order in the tetragonal cell even at very low temperatures.¹³ Weakening of the repulsive H \cdots H contacts in the cubic KBH₄, as compared to the cubic NaBH₄, is expected to be accompanied by strengthening of the metal–hydrogen (M \cdots H) interactions. The stronger K \cdots H interaction presumably determines the higher observed barrier of the BH₄ reorientational motion in KBH₄ than in NaBH₄. To underline this suggestion, we note that the shortest intermolecular H–H distances in the tetragonal NaBH₄ are not additionally shortened during the rotation of the BH₄ group around both the C₂ and the C₃ axes—they are even elongated. However, the Na–H distances become shorter on the rotation pathway, and therefore, from the mechanistic point of view, they may be responsible for creating the barrier of the BH₄ rotation. The important effect of M \cdots H interactions on the BH₄ rotation barrier is also illustrated by the fact that the contraction along the *c* axis upon the transition to the low-temperature phase leads to shorter Na–H distances and the higher energy barrier of the BH₄ jumps. H \cdots H contacts are less likely to affect the reorientational energy barrier: the H \cdots H distances in the tetragonal structure are similar to those in the cubic phase, and only their number has changed (see Figure S2 of the Supporting Information).

Another interesting conclusion on the interatomic interactions in the cubic MBH₄ series can be made from a comparison of their compressibilities. The bulk moduli for the cubic MBH₄ phases, determined in the high-pressure experiments in diamond anvil cells, decrease from the light to heavy borohydrides, going from 26(3) GPa for LiBH₄³² to 19–20 GPa for NaBH₄,^{10,33} to 16.8(4) GPa for KBH₄,³⁴ and to 14.9(4) GPa for RbBH₄.³⁵ Because the highly covalent rigid BH₄ unit is nearly incompressible compared with the H \cdots H and M \cdots H contacts, the compression of the latter two determines the compressibility. Because the H \cdots H interaction becomes weaker and the M \cdots H

interaction becomes stronger with increasing ionic radius of M and this, in turn, leads to the lower bulk modulus, we can conclude that the H \cdots H interactions primarily determine the compressibility of the cubic MBH₄.

Conclusions

The analysis of our temperature-dependent synchrotron X-ray diffraction data for NaBH₄ has shown that the transition from the low-*T* (tetragonal) to the high-*T* (cubic) phase is accompanied by a 0.4% volume increase and by a 25% increase in the volumetric expansion coefficient. The thermal expansion of the tetragonal phase is found to be anisotropic, especially close to the transition temperature. We have also revised the structure of the tetragonal phase of NaBH₄, showing that the true symmetry of this phase corresponds to the space group *P4₂/nmc*.

The analysis of the temperature and frequency dependences of the measured ¹H and ¹¹B spin–lattice relaxation rates for NaBH₄ and KBH₄ has shown that, for both compounds, the relaxation data are governed by the thermally activated reorientational motion of the BH₄ groups. The jump rates τ^{-1} of this motion derived from our data are found to change by 8 orders of magnitude over the studied temperature range of 82–424 K. The transition from the low-*T* to the high-*T* phase of NaBH₄ is accompanied by nearly an order of magnitude increase in τ^{-1} and by a considerable decrease in the activation energy E_a for the reorientational motion. The values of E_a obtained from our data are 0.151 ± 0.002 eV (low-*T* phase of NaBH₄), 0.126 ± 0.003 eV (high-*T* phase of NaBH₄), and 0.161 ± 0.002 eV (high-*T* phase of KBH₄). In the studied temperature range, we have not found any signs of distributions of the jump rates for the reorientational motion or any signs of translational diffusion on the NMR frequency scale.

Structural changes in the series of MBH₄ have been analyzed in connection with the changes in the phase-transition temperature, the compressibility, and the barrier of the reorientational BH₄ motion. On the basis of this analysis, we suggest that the reduction in the number of the repulsive H \cdots H contacts is responsible for the transition to the ordered low-temperature phase, while their compression primarily determines the compressibility. The strengthening of the M \cdots H interaction for larger M is presumably responsible for the increase in the BH₄ rotational barrier for the heavier MBH₄ compounds.

Acknowledgment. The authors are grateful to D. Chernyshov for useful discussions and to the Swiss-Norwegian Beam Lines (ESRF) for the in-house beam time allocation. This work was partially supported by the Priority Program “Basics of development of energy systems and technologies” of the Russian Academy of Sciences.

Supporting Information Available: Experimental and refined X-ray diffraction patterns for the low-temperature phase of NaBH₄ at 180 K, structural parameters for the low-temperature phase of NaBH₄, temperature dependence of the shortest H \cdots H distances between the BH₄ groups in NaBH₄, and temperature dependence of the atomic displacement parameters for NaBH₄. This material is available free of charge via the Internet at <http://pubs.acs.org>.

References and Notes

- Grochala, W.; Edwards, P. P. *Chem. Rev.* **2004**, *104*, 1283–1315.
- Orimo, S.; Nakamori, Y.; Eliseo, J. R.; Züttel, A.; Jensen, C. M. *Chem. Rev.* **2007**, *107*, 4111–4132.

- (3) Filinchuk, Y.; Chernyshov, D.; Dmitriev, V. Z. *Kristallogr.* **2008**, *223*, 649–659.
- (4) Demirci, U. B.; Miele, P. C. *R. Chim.* **2009**, *12*, 943–950.
- (5) Demirci, U. B.; Miele, P. *Energy Environ. Sci.* **2009**, *2*, 627–637.
- (6) Johnston, L.; Hallett, N. C. *J. Am. Chem. Soc.* **1953**, *75*, 1467–1468.
- (7) Stockmayer, W. H.; Stephenson, C. C. *J. Chem. Phys.* **1953**, *21*, 1311–1312.
- (8) Filinchuk, Y.; Hagemann, H. *Eur. J. Inorg. Chem.* **2008**, 3127–3133.
- (9) Fischer, P.; Züttel, A. *Mater. Sci. Forum* **2004**, *443–444*, 287–290.
- (10) Kumar, R. S.; Cornelius, A. L. *Appl. Phys. Lett.* **2005**, *87*, 261916.
- (11) Sundqvist, B.; Andersson, O. *Phys. Rev. B* **2006**, *73*, 092102.
- (12) Luck, R. L.; Schelter, E. J. *Acta Crystallogr., Sect. C* **1999**, *C55*, IUC9900151.
- (13) Renaudin, G.; Gomes, S.; Hagemann, H.; Keller, L.; Yvon, K. *J. Alloys Compd.* **2004**, *375*, 98–106.
- (14) Tsang, T.; Farrar, T. C. *J. Chem. Phys.* **1969**, *50*, 3498–3502.
- (15) Trokner, A.; Theveneau, H.; Papon, P. *J. Chem. Phys.* **1978**, *69*, 742–747.
- (16) Tarasov, V. P.; Bakum, S. I.; Privalov, V. I.; Shamov, A. A. *Russ. J. Inorg. Chem.* **1990**, *35*, 2096–2099.
- (17) Hagemann, H.; Gomes, S.; Renaudin, G. K.; Yvon, K. *J. Alloys Compd.* **2004**, *363*, 126–129.
- (18) Remhof, A.; Łodziana, Z.; Buchter, F.; Martelli, P.; Pendolino, F.; Friedrichs, O.; Züttel, A.; Embs, J. P. *J. Phys. Chem. C* **2009**, *113*, 16834–16837.
- (19) Markert, J. T.; Cotts, E. J.; Cotts, R. M. *Phys. Rev. B* **1988**, *37*, 6446–6452.
- (20) Skripov, A. V.; Rychkova, S. V.; Belyaev, M. Yu.; Stepanov, A. P. *Solid State Commun.* **1989**, *71*, 1119–1122.
- (21) Matsuo, M.; Nakamori, Y.; Orimo, S.; Maekawa, H.; Takamura, H. *Appl. Phys. Lett.* **2007**, *91*, 224103.
- (22) Skripov, A. V.; Soloninin, A. V.; Filinchuk, Y.; Chernyshov, D. *J. Phys. Chem. C* **2008**, *112*, 18701–18705.
- (23) Corey, R. L.; Shane, D. T.; Bowman, R. C.; Conradi, M. S. *J. Phys. Chem. C* **2008**, *112*, 18706–18710.
- (24) Soloninin, A. V.; Skripov, A. V.; Buzlukov, A. L.; Stepanov, A. P. *J. Solid State Chem.* **2009**, *182*, 2357–2361.
- (25) Arnbjerg, L. M.; Ravnsbæk, D. B.; Filinchuk, Y.; Vang, R. T.; Cerenius, Y.; Besenbacher, F.; Jørgensen, J.-E.; Jacobsen, H. J.; Jensen, T. R. *Chem. Mater.* **2009**, *21*, 5772–5782.
- (26) Hammersley, A. P.; Svensson, S. O.; Hanfland, M.; Fitch, A. N.; Häusermann, D. *High Pressure Res.* **1996**, *14*, 235–248.
- (27) Vogel, S.; Ehm, L.; Knorr, K.; Braun, G. *Adv. X-Ray Anal.* **2002**, *45*, 31–33.
- (28) Rodrigues-Carvajal, J. *Physica B* **1993**, *192*, 55–69.
- (29) Filinchuk, Y.; Talyzin, A.; Chernyshov, D.; Dmitriev, V. *Phys. Rev. B* **2007**, *76*, 092104.
- (30) Bürgi, H. B.; Förtsch, M. *J. Mol. Struct.* **1999**, *485–486*, 457–463.
- (31) Abragam, A. *The Principles of Nuclear Magnetism*; Clarendon Press: Oxford, U.K., 1961.
- (32) Filinchuk, Y.; Chernyshov, D.; Nevidomskyy, A.; Dmitriev, V. *Angew. Chem., Int. Ed.* **2008**, *47*, 529–532.
- (33) Chernyshov, D.; Bosak, A.; Dmitriev, V.; Filinchuk, Y.; Hagemann, H. *Phys. Rev. B* **2008**, *78*, 172104.
- (34) Kumar, R. S.; Kim, E.; Cornelius, A. L. *J. Phys. Chem. C* **2008**, *112*, 8452–8457.
- (35) Filinchuk, Y.; Talyzin, A. V.; Hagemann, H.; Dmitriev, V.; Chernyshov, D.; Sundqvist, B. *Inorg. Chem.* **2010**, to be submitted.

JP9119606